Published as: *Nat Chem Biol*. 2008 January ; 4(1): 69–74.

Discovery and characterization of a marine bacterial SAM-dependent chlorinase

Alessandra S Eustáquio[1,4], **Florence Pojer**[2,4], **Joseph P Noel**[2], and **Bradley S Moore**[1,3]

[1]Center for Marine Biotechnology and Biomedicine, Scripps Institution of Oceanography, University of California San Diego, 9500 Gilman Drive, La Jolla, California 92093, USA.

[2]Howard Hughes Medical Institute, Jack H. Skirball Center for Chemical Biology and Proteomics, The Salk Institute for Biological Studies, 10010 North Torrey Pines Road, La Jolla, California 92037, USA.

[3]Skaggs School of Pharmacy and Pharmaceutical Sciences, University of California San Diego, 9500 Gilman Drive, La Jolla, California 92093, USA.

Abstract

Halogen atom incorporation into a scaffold of bioactive compounds often amplifies biological activity, as is the case for the anticancer agent salinosporamide A (1), a chlorinated natural product from the marine bacterium *Salinispora tropica*. Significant effort in understanding enzymatic chlorination shows that oxidative routes predominate to form reactive electrophilic or radical chlorine species. Here we report the genetic, biochemical and structural characterization of the chlorinase SalL, which halogenates *S*-adenosyl-L-methionine (2) with chloride to generate 5′-chloro-5′-deoxyadenosine (3) and L-methionine (4) in a rarely observed nucleophilic substitution strategy analogous to that of *Streptomyces cattleya* fluorinase. Further metabolic tailoring produces a halogenated polyketide synthase substrate specific for salinosporamide A biosynthesis. SalL also accepts bromide and iodide as substrates, but not fluoride. High-resolution crystal structures of SalL and active site mutants complexed with substrates and products support the S_N2 nucleophilic substitution mechanism and further illuminate halide specificity in this newly discovered halogenase family.

The chlorinated marine natural product salinosporamide A (SalA, 1), a potent 20S proteasome inhibitor currently in phase 1 human clinical trials for the treatment of multiple myeloma and other cancers, is 500 times more active than its deschloro analog salinosporamide B (SalB, 5) (Fig. 1)[1–5]. The biosynthetic origin of SalA's pharmacologically active chloroethyl side chain from an unknown sugar precursor differs from the analogous ethyl group in SalB, which instead

Correspondence should be addressed to B.S.M. (bsmoore@ucsd.edu).
[4]These authors contributed equally to this work.

AUTHOR CONTRIBUTIONS

A.S.E. and F.P. contributed equally to this paper. A.S.E. performed the genetic and biochemical experiments, F.P. and A.S.E. crystallized SalL, F.P. determined the structure and performed the sedimentation velocity studies. All authors discussed the results and wrote and commented on the manuscript.

Accession codes. Protein Data Bank: The atomic coordinates and structure factors were deposited under PDB accession codes 2Q6I, 2Q6K, 2Q6O and 2Q6L for SalL wild-type complex with 5′-ClDA and L-methionine, SalL wild-type complex with adenosine, SalL Y70T complex with chloride and SAM, and SalL Y70T G131S complex with 5′-ClDA and L-methionine, respectively. *S. cattleya* fluorinase structures were deposited as part of previous studies under PDB codes 1RQP and 2C2W.

Note: Supplementary information and chemical compound information is available on the Nature Chemical Biology website.

originates from butyrate (6)[6]. Analysis of the 41-kilobase *sal* biosynthetic gene cluster from *S. tropica* revealed a polyketide synthase–nonribosomal peptide synthetase (PKS-NRPS) hybrid pathway involving a new chlorination route for SalA production[7]. None of the previously described oxidative chlorinating enzyme–coding genes[8] are present in the *sal* locus. Rather, we identified the gene *salL*, whose protein product is homologous to the fluorinase FlA (35% amino acid identity) from the soil bacterium *S. cattleya*[9]. FlA catalyzes the fluoride-dependent nucleophilic displacement of L-methionine (4) from *S*-adenosyl-L-methionine (SAM, 2) to generate 5′-fluoro-5′-deoxyadenosine (5′-FDA, 7) as the first step in the biosynthesis of fluoroacetate (8) (Fig. 1a)[9,10].

Here we report the *in vivo* and *in vitro* characterization of SalL as a new chlorinating enzyme that functions in an orthogonal manner to biological chlorination reactions to initiate the biosynthesis of a new halogenated PKS building block.

RESULTS

In vivo functional analysis of *salL*

The 849-base-pair gene *salL* was inactivated by PCR-targeted mutagenesis to explore the possibility that its product SalL serves as a chlorinase that catalyzes the synthesis of the dedicated pathway intermediate 5′-chloro-5′-deoxyadenosine (5′-ClDA, 3) from the primary metabolite SAM. Further processing of the 5′-ClDA ribose unit would then provide the chlorinated PKS extender unit uniquely required for SalA assembly (Fig. 1a). Fermentation of the resulting *salL*$^{-}$ mutant strain revealed the selective loss of SalA in cultures still producing SalB (Fig. 1c) via butyrate incorporation by way of ethylmalonyl coenzyme A (9) (Fig. 1b). Chemical complementation of the *salL*$^{-}$ mutant strain with 5′-ClDA selectively restored SalA production (Fig. 1c), thereby confirming the metabolic intermediacy of 5′-ClDA, in which the chlororibose unit gives rise to the ‘chlorobutyrate’ PKS building block in SalA, presumably via the new metabolite chloroethylmalonyl coenzyme A (10) (Fig. 1a).

Biochemical characterization of SalL as a 5′-ClDA synthase

SalL behaves as a soluble (60 mg l^{-1}) trimeric protein (30 kDa per monomer of 283 residues) when purified from *Escherichia coli* BL21(DE3). In the presence of SAM, recombinant SalL showed a surprising flexibility for the halides chloride, bromide and iodide, producing halogenated 5′-deoxyadenosine (5′-XDA) and L-methioine. Notably, no halogenase activity was detected in the presence of fluoride using either standard assays or coupled-enzyme assays in which coproduced L-methionine was oxidized with L-amino acid oxidase to inhibit the reverse reaction[11]. Apparent steady state kinetic constants of SalL were measured *in vitro* by monitoring the formation of either 5′-XDA (forward reaction) or SAM (reverse reaction) (Table 1). Although the affinity of SalL for SAM (K_m 1 μM) is much higher than that of chloride (K_m 45 mM), seawater has a chloride concentration of 546 mM. The brominase and iodinase activities are probably not biologically relevant in this marine bacterium given the low concentration of these halides in seawater (0.8 mM bromide and 0.5 μM iodide, which are 187 and 520,000 times less than K_m, respectively). Replacement of synthetic sea salt with sodium bromide in the *S. tropica* fermentation medium results in the *in vivo* production of bromosalinosporamide (11)[12], which further illuminates the broad halide promiscuity of the *sal* PKS in accepting a range of biosynthetic building blocks.

The relative enzyme efficiency (k_{cat}/K_m) shows that the reverse reaction (formation of SAM) is several orders of magnitude more efficient *in vitro* than the forward halogenase reaction (Table 1). This is especially noteworthy with 5′-IDA (12) and its softer halide leaving group. In comparison, 5′-FDA is not a substrate, which likely corresponds to the high energy necessary to cleave the C–F bond[11,13]. Because the reaction proceeds *in vitro* in the absence of other

metabolic pathway enzymes in favor of substrates, the subsequent biosynthetic enzyme, purine nucleoside phosphorylase SalT (FlB in *S. cattleya*[10]), may be important to pull the equilibrium toward 5′-ClDA formation and ultimately SalA (Fig. 1a). The reaction equilibrium also ensures that SAM will be committed to secondary metabolite production only as needed.

Structural basis for substrate specificity and mechanism in SalL

We next determined several high-resolution X-ray crystal structures of wild-type SalL and active site mutants complexed with substrates and products (Supplementary Table 1 online). SalL organizes as a homotrimer whose monomeric units (r.m.s. deviation = 1.8 Å) resemble the two-domain structure of fluorinase (Protein Data Bank (PDB) entry 1RQP) (Fig. 2a). The active site of these two evolutionarily related enzymes resides at the interface of adjacent monomers with three active sites per trimer. Sedimentation velocity studies confirmed that SalL forms a trimer in solution (Supplementary Fig. 1 online) in contrast to fluorinase, which was shown by gel filtration to be hexameric (dimer of trimers)[9]. Though similar architecturally, SalL differs from fluorinase by the absence of a 23-residue loop inserted in the N-terminal domain between residues 87 to 90 (of SalL). The loss of this extended loop in SalL decreases the buried surface area around the active site of SalL relative to fluorinase.

When *salL* was expressed using culture medium low in chloride, the protein copurified with adenosine (13) and 5′-ClDA in a 35:1 molar ratio as measured by HPLC. On addition of 250 mM NaCl to the *E. coli* culture medium, recombinant SalL copurified with 80% 5′-ClDA occupancy. Inspection of $F_o - F_c$ electron density maps for refined complexes with 5′-ClDA showed no extraneous difference density. Moreover, the refined *B*-factors for the chlorine atom of 5′-ClDA are the same or less than those for surrounding protein, ligand and water atoms, again providing very strong circumstantial support for the presence of 5′-ClDA in the described complex. The second product of the reaction, L-methionine, exhibited partial occupancy in the active site, and in contrast to the fluorinase, interacted only with C-terminal residues resembling a loosely held product complex (Fig. 2b). Analogous to 5′-FDA and 5′-ClDA in fluorinase (PDB codes 1RQP and 2C2W, respectively)[9,11], 5′-ClDA is well sequestered and buried in the SalL active site with conserved hydrogen bonds between Asp11 (Asp16 in fluorinase) and the 2′- and 3′-OHs of the ribose moiety, and between Asn188 (Asn215 in fluorinase) and the adenine ring (Fig. 2b). Notably, Ser158 (position 131 in SalL) in fluorinase is replaced by a glycine in SalL. The Ser158 side chain was proposed to offset the energetic cost of desolvation of fluoride through compensatory hydrogen bonding. This difference results in a larger pocket in SalL compared with fluorinase[9], and this increased halide binding pocket matches the halide discrimination of SalL for larger ionic radii (chloride, 1.67 Å; bromide, 1.82 Å; iodide, 2.06 Å; versus fluoride, 1.19 Å).

The well-defined electron density of the product reveals polar contacts between the backbone amide of Gly131 and the 5′-ClDA chlorine atom (3.1 Å).Moreover, the chlorine atom is displaced relative to the location of the corresponding organohalogen bound to fluorinase. The substitution of an extended hydrogen bond donor side chain for a hydrogen bonding backbone amide (Ser158 in fluorinase versus Gly131 in SalL) may partially explain the inability of SalL to desolvate the fluoride anion and catalyze C-F bond formation.

Replacement of Gly131 with a serine led to the loss of SalL halogenase activity and the inability to crystallize G131S SalL. Other notable differences between SalL and fluorinase within 4 Å of Gly131 include Tyr70, which is replaced by Thr77 in fluorinase. The Y70T SalL mutation results in a two-orders-of-magnitude reduction of SalL activity (Table 1). Structurally, SalL Y70T provided a high-resolution view of SAM and chloride bound in the active site (Fig. 2c). Assignment of chloride rather than water is supported by the geometry of the anion's hydrogen bonding arrangement, the absence of negative or positive electron density above background in $F_o - F_c$ maps, and the refined *B*-factor of the chloride anion (12 $Å^2$) compared with

surrounding atoms (>15 $Å^2$). Though it is difficult to distinguish fluoride from a bound water given that they have a similar number of scattering electrons, chloride has substantially more scattering electrons and is therefore relatively easy to identify crystallographically from refined electron density maps and its associated *B*-factor.

The chloride anion is hydrogen bonded to two water molecules and the backbone amide of Gly131 (2.8 Å). In contrast to wild-type SalL or fluorinase, the Y70T mutation affords water access to the active site with concomitant solvation of the halide ion, thereby inhibiting halogenase activity. Moreover, the theoretical angle of 180° between the chloride ion and the S^+-C bond of SAM (Fig. 2d) is consistent with an S_N2-type mechanism as reported for fluorinase[14]. Tyr70 (Fig. 2b) is in turn hydrogen bonded to Trp129 (Phe156 in fluorinase). The W129F mutant of SalL has reduced activity, however, to a much lesser extent than the Y70T mutant (Table 1). Based on the previously reported fluorinase structure and the structure of SalL reported here, it seems that these nucleophilic halogenases acquired their halogenating catalytic machinery at least in part by excluding water from the active site to "activate" halide anions for nucleophilic displacement reactions.

Most important, the double mutant Y70T G131S SalL shows four to five times increased chlorinating and brominating activity compared with the compromised Y70T single mutant. The combination of both mutations resulted in crystallizable protein and elucidation of the Y70T G131S mutant structure. Unlike the Y70T SalL structure, the SalL Y70T G131S structure complexed with products shows an active site free of water, thus again favoring the nucleophilic substitution reaction due to halide desolvation (Fig. 3a). The inability of the SalL Y70T G131S double mutant to iodinate correlates with the constriction of the halide binding pocket by the G131S replacement. Furthermore, despite mutations toward a more "fluorinase"-like protein, no enzymatic activity was detected in the presence of fluoride. A structural overlay of SalL Y70T G131S and fluorinase highlights a subtle 1.4-Å displacement of the loop carrying Ser131 (SalL numbering) away from the product relative to the fluorinase structure (Fig. 3b). This displacement results in a disruption of the hydrogen bonding network involving Ser131 and the 2′-OH of the ribose (3.82 Å in SalL versus 2.7 Å in fluorinase), the halide of 5′-XDA and the interaction with Thr70. In fact, the additional 23-residue loop in the N-terminal domain of fluorinase sits just above the active site and appears to compress the loop carrying this catalytic serine residue, thus enabling its contact with the ribose unit and Thr75 in fluorinase (Fig. 3b,c). The absence of this extra loop in SalL modifies the active site architecture and residue-product interactions, thereby influencing its halide specificity due to subtle rearrangements of the halide binding pocket.

DISCUSSION

In conclusion, the mode of chlorine incorporation by SalL is mechanistically orthogonal to recent examples of natural product chlorination that predominate via oxidative routes. The subsequent metabolism of 5′-ClDA to the putative PKS extender unit chloroethylmalonyl coenzyme A and its assimilation into the hybrid PKS-NRPS product salinosporamide A is to our knowledge an unprecedented mode of organohalogen assimilation and affords new opportunities for the rational engineering of halogenated polyketides. As far as we know, the only other nucleophilic chlorination reaction described so far involves the SAM-dependent methylation of chloride to form methylchloride[15–17]. Although this reaction is mechanistically analogous to those of fluorinase and SalL, it uses distinct enzymes whose biological relevance remains to be demonstrated. Moreover, whereas methylchloride is limited in downstream metabolic utility, the SalL product 5′-ClDA is exquisitely designed to enter a multitude of metabolic pathways that may be of biotechnological value.

METHODS

Chemicals

SAM-*p*-toluenesulfonate, L-methionine and 5′-ClDA were from Sigma. 5′-IDA was from Acros Organics. 5′-FDA and 5′-BrDA (14) were a gift (see Acknowledgments). All other chemicals were of analytical grade.

salL knockout and secondary metabolite analysis

salL was inactivated using the PCR-targeting system with some modifications[18]. After PCR amplification of the apramycin resistance (*aac(3)IV*) cassette from pIJ773 using primers P1-salL (5′-GTCGGTTTCCGACCGATAAAACGGAGGTCACTCACCATGAT TCCGGGATCCGTCGACC-3′) and P2-salL (5′-AGGAGCTACCCAGCAGCATG CCGCCCCCTGGGTCAGCTATGTAGGCTGGAGCTGCTTC-3′), the extended cassette was introduced into *E. coli* BW25113/pKD20 (ref. [19]), containing fosmid BHXS3930, which included the *sal* biosynthetic gene cluster (ref. [7]). The mutated fosmid was then introduced into *S. tropica* CNB-440 by conjugation from *E. coli* S17-1, and gene replacement was confirmed by Southern blot analysis and PCR. For analysis of secondary metabolites, mutant and wild-type strains of *S. tropica* were cultured in 50 ml of natural seawater-based medium as described[6]. HPLC analysis of the crude extract was carried out with a Phenomenex C18 column (150 × 4.6 mm; 5 μm particle size) at a flow rate of 0.7 ml min^{-1} using isocratic 35% acetonitrile in water as the mobile phase with detection at 210 nm. SalA and SalB identities were confirmed with authentic standards and by LC/(+)ESI-MS (refs. [1,3]).

SalL purification

The *salL* gene from *S. tropica* CNB-440 was amplified by PCR from total genomic DNA using the forward primer 5′-CGTGGTTCCCATGGCATGCAGCACAATCTCATTGC-3′ (*Nco*I site underlined) and the reverse primer 5′-GCTCGAATTCAAGCTTGTCAGCTACCC GAGCACCG-3′ (*Hin*dIII site underlined), designed for ligation into pHIS8 (ref. [20]), yielding plasmid pAEM7. Expression in *E. coli* BL21(DE3), purification and removal of the N-terminal His_8 tag were carried out as previously described[20] but with the following modifications: growth was carried out at 25 °C until A_{600} = 0.8; after induction with 0.25 mM IPTG, cells were cultured overnight at 20 °C; Tris-HCl buffers containing NaCl were replaced by phosphate buffers with Na_2SO_4. The yield was 60 mg soluble protein per liter of culture. The SalL quaternary structure was determined by sedimentation velocity experiments conducted with an Optima XLI centrifuge (Beckman Coulter) using an An50 Ti eight-hole rotor. Epon double-sector centerpieces were filled with 400 μl of samples containing purified SalL at different concentrations. Samples were centrifuged at 42,000 r.p.m. at 20 °C, and data were collected by absorbance at 280 nm. Sedimentation velocity analyses were performed with SEDFIT (http://www.analyticalultracentrifugation.com) as previously described[21]. All mutants were generated using the QuickChange (Stratagene) PCR-based method. Mutant enzymes were purified as described above for the wild type. The protein yield was comparable to the wild type for all mutants, except Y70T, which showed about a ten-fold reduction in protein yield.

SalL activity assay

SalL reactions were investigated by incubating the enzyme (10 to 300 nM) with (i) 0.5–500 μM SAM and 10–500 mM KX (X = F, Cl, Br, I) or (ii) 0.5–100 mM L-methionine and 0.3–100 μM 5′-XDA (X = F, Cl, Br, I) in 50 mM phosphate buffer (pH 7.9) at 37 °C. After boiling the reaction mixture for 2 min and centrifuging for 30 min to eliminate precipitated protein, 10–100 μl of the clear supernatant was analyzed by HPLC as described[22]. The identity of

products was confirmed by comparing the retention times with authentic standards and by LC/(+)ESI MS. The detection limit of the HPLC assay was >1 pmol.

Crystallization, data collection and structure determination

Crystals were obtained by vapor diffusion at 4 °C by equilibrating 2 μl hanging drops containing a 1:1 mixture of 10 mg ml^{-1} protein and crystallization buffer (28% (w/v) PEG 3350, 0.3 M KCl, 2 mM DTT, 0.1 M MOPSO, pH 7.0) over a 500 μl reservoir of the same crystallization solution. Crystals were stabilized by soaking briefly in a cryoprotectant solution (25% ethylene glycol (w/v) in crystallization buffer) and flash frozen in liquid nitrogen before data collection. The SalL wild-type complex with 5′-ClDA was obtained by overnight soaking of crystals in 2 μl crystallization drops containing 10 mM 5′-ClDA. SalL Y70T copurified with SAM, and chloride was present in the crystallization buffer. Diffraction data were collected on BL8.2.2 at the Advanced Light Source. Data were indexed, integrated and scaled with X-ray detector software (XDS) (ref. [23]). SalL wild-type and double-mutant Y70T G131S crystallized in the $P6_322$ space group with unit cell dimensions of approximately $a = b = 111$ Å, $c = 95$ Å, $\alpha = \beta = 90°$ and $\gamma = 120°$, with one molecule in the asymmetric unit (Supplementary Table 1). Phase determination was carried out by molecular replacement using MOLREP (ref. [24]), part of the CCP4 Suite[25]. We used as a search model the published structure of *S. cattleya* fluorinase (PDB accession number 1RQP)[9]. The initial molecular replacement models were manually adjusted in COOT, part of the CCP4 package[25] and refined with REFMAC5 (ref. [26]). SalL single-mutant Y70T crystallized in the *P*3 space group with unit cell dimensions of approximately $a = b = 111$ Å, $c = 47$ Å, $\alpha = \beta = 90°$ and $\gamma = 120°$, with two molecules in the asymmetric unit (Supplementary Table 1). SalL Y70T data was twinned (twinning operator of $h, -h-k, -l$ and twinning fraction of 0.304) and was therefore refined as twinned data in CNS (http://cns.csb.yale.edu/v1.2/). A summary of the final refinement statistics is available in Supplementary Table 1. The refined structures were evaluated with PROCHECK (ref. [27]). 0–0.5% unfavorable geometries were found and >87% of residues were in the "most favored" conformation. Structure figures were prepared with PyMOL (ref. [28]).

Supplementary Material

Refer to Web version on PubMed Central for supplementary material.

ACKNOWLEDGMENTS

We kindly thank D. O'Hagan (University of St. Andrews) for providing 5′-FDA and 5′-BrDA standards, B. Gust and Plant Bioscience Limited for the REDIRECT technology kit for PCR targeting, A. Lapidus (Joint Genome Institute) for fosmid BHXS3930 and R. McGlinchey for valuable discussions. A.S.E. is a Tularik postdoctoral fellow of the Life Sciences Research Foundation, and F.P. is a Deutsche Forschungsgemeinschaft postdoctoral fellow. This work was supported by grants from the US National Oceanic and Atmospheric Administration (NA05NOS4781249 to B.S.M.), the US National Institutes of Health (CA127622 to B.S.M.) and the US National Science Foundation (MCB-023602 to J.P.N.). J.P.N. is an investigator of the Howard Hughes Medical Institute.

References

1. Feling RH, et al. Salinosporamide A: a highly cytotoxic proteasome inhibitor from a novel microbial source, a marine bacterium of the new genus *Salinospora*. Angew. Chem. Int. Edn. Engl 2003;42:355–357.
2. Maldonado LA, et al. *Salinispora arenicola* gen. nov., sp. nov. and *Salinispora tropica* sp. nov., obligate marine actinomycetes belonging to the family Micromonosporaceae. Int. J. Syst. Evol. Microbiol 2005;55:1759–1766. [PubMed: 16166663]
3. Williams PG, et al. New cytotoxic salinosporamides from the marine actinomycete *Salinispora tropica*. J. Org. Chem 2005;70:6196–6203. [PubMed: 16050677]

4. Voorhees PM, Dees EC, O'Neil B, Orlowski RZ. The proteasome as a target for cancer therapy. Clin. Cancer Res 2003;9:6316–6325. [PubMed: 14695130]
5. Chauhan D, et al. A novel orally active proteasome inhibitor induces apoptosis in multiple myeloma cells with mechanisms distinct from Bortezomib. Cancer Cell 2005;8:407–419. [PubMed: 16286248]
6. Beer LL, Moore BS. Biosynthetic convergence of salinosporamides A and B in the marine actinomycete *Salinispora tropica*. Org. Lett 2007;9:845–848. [PubMed: 17274624]
7. Udwary DW, et al. Genome sequencing reveals complex secondary metabolome in the marine actinomycete *Salinispora tropica*. Proc. Natl. Acad. Sci. USA 2007;104:10376–10381. [PubMed: 17563368]
8. Vaillancourt FH, Yeh E, Vosburg DA, Garneau-Tsodikova S, Walsh CT. Nature's inventory of halogenation catalysts: oxidative strategies predominate. Chem. Rev 2006;106:3364–3378. [PubMed: 16895332]
9. Dong C, et al. Crystal structure and mechanism of a bacterial fluorinating enzyme. Nature 2004;427:561–565. [PubMed: 14765200]
10. Huang F, et al. The gene cluster for fluorometabolite biosynthesis in *Streptomyces cattleya*: a thioesterase confers resistance to fluoroacetyl-coenzyme A. Chem. Biol 2006;13:475–484. [PubMed: 16720268]
11. Deng H, et al. The fluorinase from *Streptomyces cattleya* is also a chlorinase. Angew. Chem. Int. Edn. Engl 2006;45:759–762.
12. Lam KS, et al. Effects of halogens on the production of salinosporamides by the obligate marine actinomycete *Salinispora tropica*. J. Antibiot. (Tokyo) 2007;60:13–19. [PubMed: 17390584]
13. Harper DB, O'Hagan D. The fluorinated natural products. Nat. Prod. Rep 1994;11:123–133. [PubMed: 15209126]
14. Cadicamo CD, Courtieu J, Deng H, Meddour A, O'Hagan D. Enzymatic fluorination in *Streptomyces cattleya* takes place with an inversion of configuration consistent with an S_N2 reaction mechanism. ChemBioChem 2004;5:685–690. [PubMed: 15122641]
15. Wuosmaa AM, Hager LP. Methyl chloride transferase: a carbocation route for biosynthesis of halometabolites. Science 1990;249:160–162. [PubMed: 2371563]
16. Ni X, Hager LP. cDNA cloning of *Batis maritima* methyl chloride transferase and purification of the enzyme. Proc. Natl. Acad. Sci. USA 1998;95:12866–12871. [PubMed: 9789006]
17. Ni X, Hager LP. Expression of *Batis maritima* methyl chloride transferase in *Escherichia coli*. Proc. Natl. Acad. Sci. USA 1999;96:3611–3615. [PubMed: 10097085]
18. Gust B, Challis GL, Fowler K, Kieser T, Chater KF. PCR-targeted *Streptomyces* gene replacement identifies a protein domain needed for biosynthesis of the sesquiterpene soil odor geosmin. Proc. Natl. Acad. Sci. USA 2003;100:1541–1546. [PubMed: 12563033]
19. Datsenko KA, Wanner BL. One-step inactivation of chromosomal genes in *Escherichia coli* K-12 using PCR products. Proc. Natl. Acad. Sci. USA 2000;97:6640–6645. [PubMed: 10829079]
20. Jez JM, Ferrer JL, Bowman ME, Dixon RA, Noel JP. Dissection of malonyl-coenzyme A decarboxylation from polyketide formation in the reaction mechanism of a plant polyketide synthase. Biochemistry 2000;39:890–902. [PubMed: 10653632]
21. Dam J, Schuck P. Calculating sedimentation coefficient distributions by direct modeling of sedimentation velocity concentration profiles. Methods Enzymol 2004;384:185–212. [PubMed: 15081688]
22. Schaffrath C, Deng H, O'Hagan D. Isolation and characterisation of 5′-fluorodeox-yadenosine synthase, a fluorination enzyme from *Streptomyces cattleya*. FEBS Lett 2003;547:111–114. [PubMed: 12860396]
23. Kabsch, W. Ch. 11.3. In: Rossman, MG.; Arnold, E., editors. International Tables for Crystallography. Netherlands: Kluwer Academic Publisher Dordrecht; 2001.
24. Vagin AA, Isupov MN. Spherically averaged phased translation function and its application to the search for molecules and fragments in electron-density maps. Acta Crystallogr. D Biol. Crystallogr 2001;57:1451–1456. [PubMed: 11567159]
25. Collaborative Computational Project. Number 4. The CCP4 suite: programs for protein crystallography. Acta Crystallogr. D Biol. Crystallogr 1994;50:760–763. [PubMed: 15299374]

26. Vagin AA, et al. REFMAC5 dictionary: organization of prior chemical knowledge and guidelines for its use. Acta Crystallogr. D Biol. Crystallogr 2004;60:2184–2195. [PubMed: 15572771]

27. Laskowski RA. Structural quality assurance. Methods Biochem. Anal 2003;44:273–303. [PubMed: 12647391]

28. DeLano, WL. The PyMOL Molecular Graphics System. California, USA: DeLano Scientific, San Carlos; 2002.

29. Akopiants K, Florova G, Li C, Reynolds KA. Multiple pathways for acetate assimilation in *Streptomyces cinnamonensis*. J. Ind. Microbiol. Biotechnol 2006;33:141–150. [PubMed: 16187095]

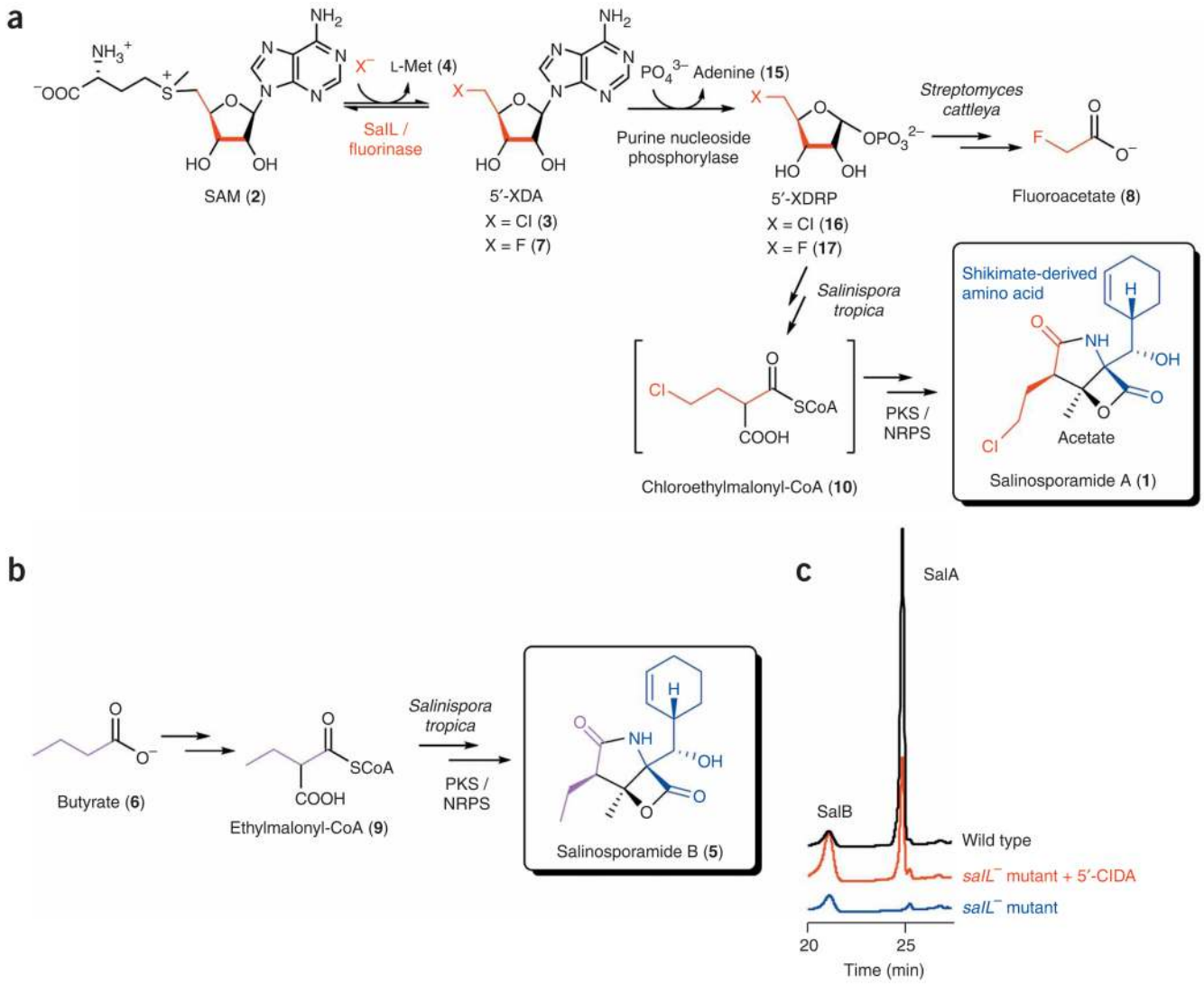

Figure 1. Biosynthesis and structures of salinosporamides A and B

(**a**) Proposed common steps for the biosynthesis of fluoroacetate by *S. cattleya* and of the chlorinated unit of salinosporamide A by *S. tropica*. The origin of the carbons is color coded[8]. L-Met, L-methionine. (**b**) Butyrate as a precursor of salinosporamide B can originate from several pathways for acetate assimilation and fatty acid or polyketide biosynthesis[29]. (**c**) HPLC chromatograms of culture extracts of *S. tropica* wild type, the *salL*⁻ mutant strain constructed by gene replacement with an apramycin resistance marker via PCR tartgeting[18], and the *salL*⁻ mutant strain supplemented with 5′-ClDA.

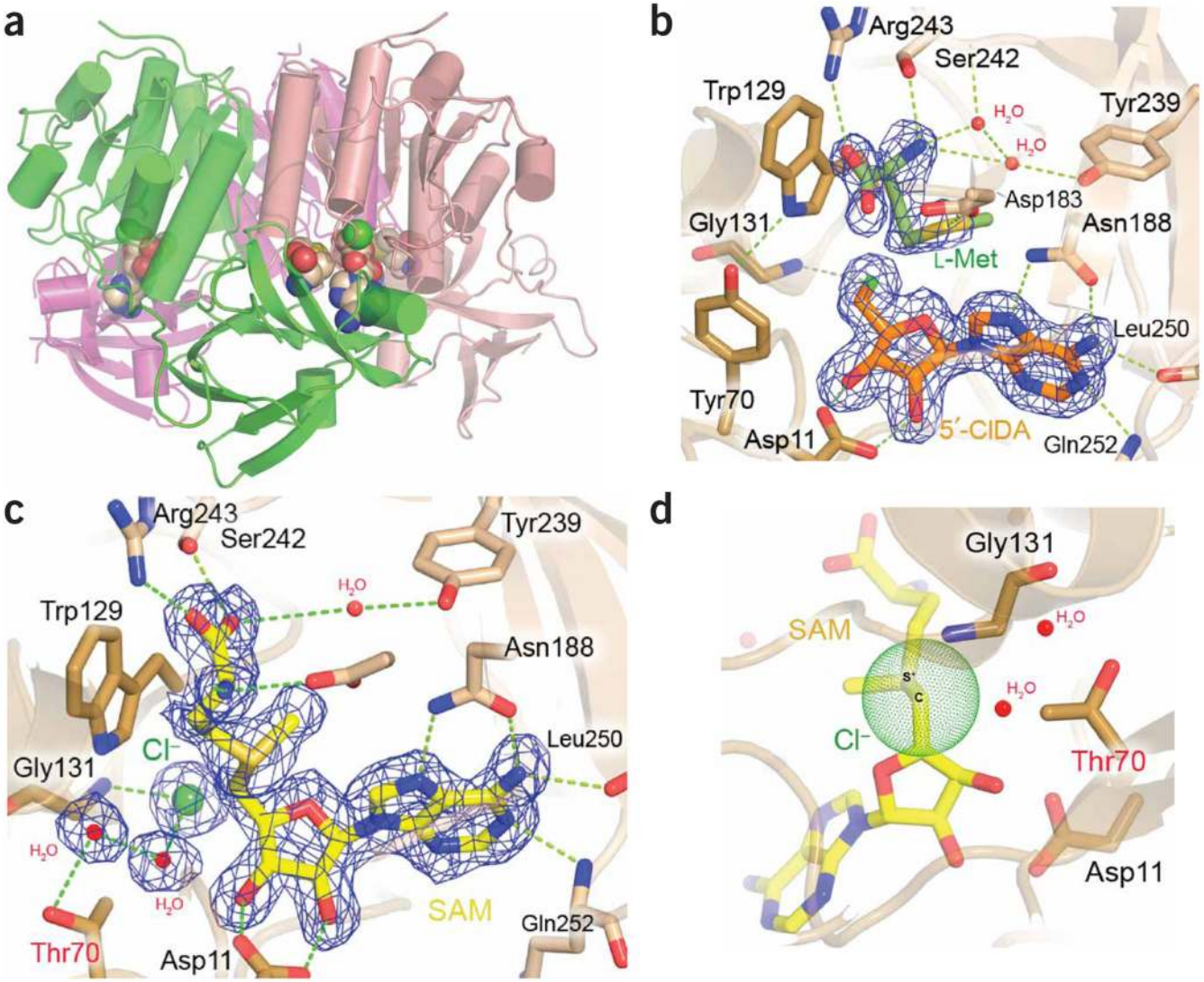

Figure 2. Structures of wild-type SalL and the Y70T mutant

(**a**) Overall architecture of homotrimeric SalL with bound 5′-ClDA and L-methionine located at the interface of adjacent monomers. (**b**) Close-up view of the active site of wild-type SalL with bound products 5′-ClDA and L-methionine. The SIGMAA-weighted $2F_o - F_c$ electron density map is shown in blue contoured at 1σ. Hydrogen bonds are depicted as green dashes. Waters are shown as red dots. Residues from the C-terminal region of monomer A are colored dark gold, and those from the N-terminal region of monomer B are colored off-white. 5′-ClDA is hydrogen bonded to monomer A (Cl atom to the amide backbone of Gly131, and the 2′-OH and 3′-OH of ribose to Asp11) and to monomer B (adenine ring to Asn188), while L-methionine forms hydrogen bonds to only monomer B (Ser142 and Arg243). (**c**) Close-up view of the active site of Y70T SalL with the trapped substrates Cl^- and SAM. Cl^- forms hydrogen bonds with the amide backbone of Gly131 as well as two newly observed water molecules that most likely reduce the nucleophilicity of Cl^- to impede the forward S_N2 displacement reaction. (**d**) Reorientation of **c** illustrating the nearly 180° angle between the incoming Cl^- and the S^+-C σ bond of SAM typical of an S_N2-type reaction mechanism.

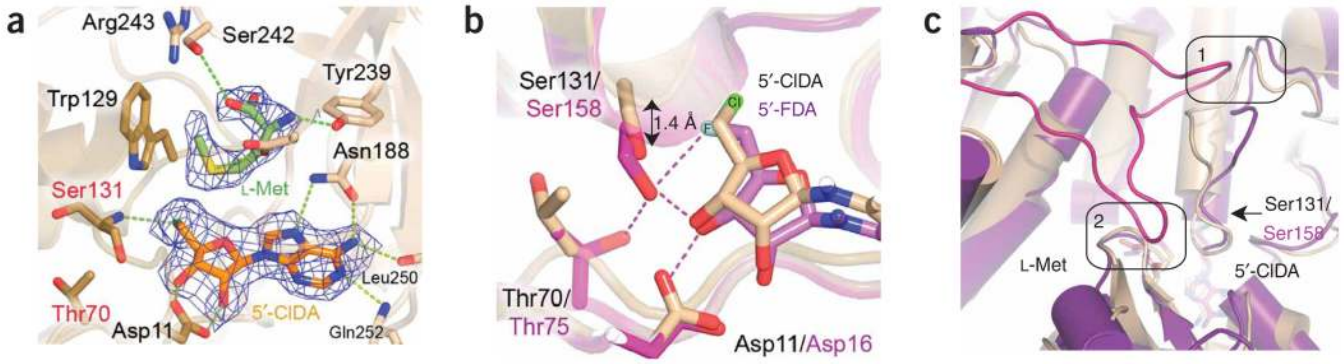

Figure 3. SalL double-mutant Y70T G131S and structural comparison with fluorinase

(**a**) Close-up view of the active site of SalL Y70T G131S with bound 5′-ClDA and L-methionine. The SIGMAA-weighted $2F_o - F_c$ electron density map is shown in blue contoured at 1σ. Hydrogen bonds are depicted as green dashes. The chlorine atom forms hydrogen bonds to the amide backbone of Ser131. Unlike the Y70T point mutant structure, no water molecules are observed in the active site, as in wild-type SalL. (**b**) Overlay of the active sites of SalL Y70T G131S (off-white) and fluorinase (purple) (PDB code 1RQP). In fluorinase, Ser158 forms a hydrogen bonding network with Thr75, the 2′-OH of the ribose, and the fluorine atom of 5′-FDA. The loop harboring Ser131 in the chlorinase SalL Y70T G131S is displaced by 1.4 Å relative to the equivalent loop harboring Ser158 in fluorinase, thereby disrupting the hydrogen bonding network. (**c**) Overlay of SalL Y70T G131S (off-white) and fluorinase (purple) with the N-terminal region of fluorinase containing the inserted fluorinase loop (pink) that interacts with the N-terminal region of the adjacent monomer (domain 1, backbone amide nitrogen of Gly107 hydrogen bonds to the carbonyl of Pro145 and the carbonyl of Ile148; and the carbonyl of Gly107 hydrogen bonds to the backbone amide nitrogen of Glu150) and packs itself (Gly98 and Ala99) against the C-terminal region (Ser269 to Gly271) of the same monomer (domain 2) and hence compresses the loop carrying Ser158.

Table 1

Apparent kinetic constants of SalL wild type and relative activity of point mutants

Substrate	k_{cat} (min^{-1})	Relative activity (%)[a]	K_m (mM)	k_{cat}/K_m (mM^{-1} min^{-1})
Forward reaction				
SAM	0.9 ± 0.1	100	$(1 \pm 0.2) \times 10^{-3}$	900
F^-	n.d.	n.d.	n.d.	n.d.
Cl^-	0.9 ± 0.1	100	45 ± 5	0.02
Br^-	0.8 ± 0.1	90	150 ± 15	0.0053
I^-	0.3 ± 0.1	33	260 ± 20	0.00115
Reverse reaction				
L-Met	12 ± 1	1,300	2.6 ± 0.2	4.6
5′-FDA	n.d.	n.d.	n.d.	n.d.
5′-ClDA	12 ± 1	1,300	$(2 \pm 1) \times 10^{-4}$	60,000
5′-BrDA	a.d.	a.d.	a.d.	a.d.
5′-IDA	50 ± 5	5,555	$(4.6 \pm 0.1) \times 10^{-3}$	10,869

Relative activity[a] of SalL point mutants

	Substrate				
SalL	Cl^-	Br^-	I^-	5′-ClDA	5′-IDA
Wild type	100%	100%	100%	100%	100%
W129F	52%	76%	3%	11%	12%
G131S	n.d.	n.d.	n.d.	n.d.	n.d.
Y70T	0.07%	0.1%	0.4%	1.1%	1.4%
Y70T G131S	0.3%	0.5%	n.d.	2.5%	0.8%

The kinetic values are average of at least two independent measurements. For comparison, the kinetic constants reported for fluorinase are: K_m for F^- of 2 mM and for SAM of 74 μM, k_{cat} 0.007 min^{-1} for the forward reaction with the equilibrium lying in favor of 5′-FDA by a factor of three, and the rate preference for F^- over Cl^- by a factor of 120 (refs. [9,11]). n.d., activity not detected; a.d., activity detected, however, kinetic constants were not determined because of unavailability of sufficient substrate.

[a] Relative activity is based on k_{cat} values.